Computer Physics Communications 181 (2010) 1037–1046

Contents lists available at ScienceDirect

Computer Physics Communications

www.elsevier.com/locate/cpc

A phase-field approach for minimizing the area of triply periodic surfaces with volume constraint

Seong-Deog Yang, Hyun Geun Lee, Junseok Kim *

Department of Mathematics, Korea University, Seoul 136-701, Republic of Korea

ARTICLE INFO

Article history:
Received 31 July 2009
Received in revised form 3 February 2010
Accepted 15 February 2010
Available online 19 February 2010

Keywords:
Phase-field model
Unconditionally gradient stable scheme
Constant mean curvature

ABSTRACT

In this paper, we present an accurate and efficient algorithm to generate constant mean curvature surfaces with volume constraint using a phase-field model. We implement our proposed algorithm using an unconditionally gradient stable nonlinear splitting scheme. Starting from the periodic nodal surface approximation to minimal surfaces, we can generate various constant mean curvature surfaces with given volume fractions. We generate and study the Schwarz primitive (P), Schwarz diamond (D), and Schoen gyroid (G) surfaces with various volume fractions. This technique for generating constant mean curvature surfaces can be used to design biomedical scaffolds with optimal mechanical and biomorphic properties.

1. Introduction

A minimal surface is a surface for which the mean curvature H is zero at every point [4]. A remarkable class of minimal surfaces are triply periodic (i.e., periodic in three directions). The Schwarz primitive (P), the Schwarz diamond (D), and the Schoen gyroid (G) minimal surfaces partition space into two disjoint but congruent regions, hence the volume fraction of each phase is 1/2 (see Fig. 1).

Triply periodic minimal surfaces [20–22] offer great attractions to physical scientists, biologists, and mathematicians. In forming an equilibrium structure, such a material may separate into distinct phases, creating domains of component A and component B. Lipid–water systems are known to display cubic phases that are bicontinuous; i.e., the entire aqueous region is divided by the lipid bilayer into two disconnected regions that are simultaneously continuous. The bilayer has been shown to be an infinite periodic minimal surface [16]. Cell membranes resembling periodic minimal surfaces have been observed in cytoplasmic organelles such as mitochondria and chloroplasts [24]. It has been suggested that in certain invertebrates the endoplasmic reticulum (a system of interconnecting membranes inside the cell) may exhibit gyroid (spiral) cubic structures. The geometry of triply periodic minimal surfaces strongly influences the physical properties of the material and they have been proposed as candidates for microstructural models in a variety of physical and biological systems. Dominant factors in the determination of the domain morphology are area-minimization of interface and a triply-periodic condition, subject to fixed volume fraction.

Recently, it was shown that triply periodic minimal surfaces can be generated as the local minima of the scalar order parameter Landau–Ginzburg functional for describing ordering phenomena in microemulsion. This Landau–Ginzburg free energy functional can be utilized to calculate numerically a discretization of a potential $\phi(x)$ such that $\phi(x) > 1/2$ for points in phase 1 and $\phi(x) < 1/2$ for points in phase 2. At the phase interface, $\phi(x) = 1/2$, which in this case is the Schwarz P, Schwarz D, or Schoen G minimal surface. Moreover, the minimal surfaces can be approximated by the periodic nodal surface (PNS) of a sum defined in terms of the Fourier series, because any periodic surface can be expressed as the sum of an infinite number Fourier terms [10].

There are many approaches to generate discrete triply periodic minimal surfaces. In [17], Jung, Chu, and Torquato explored triply periodic surfaces with minimal surface area under a constraint in the volume fraction of the phases that the surface separates using the level set method [1,26,27,32]. In [23], Mackay constructed periodic minimal surfaces using the concept of nodal and Fermi surfaces. Brakke [2] developed the Surface Evolver and the Surface Evolver is a computer program that minimizes the energy of a surface subject to constraints. The authors in [13,28,33] studied triply periodic minimal surfaces using the Surface Evolver. In the fields of CAD, Wang [36] proposed a periodic surface modeling scheme that can approximate triply periodic minimal surfaces and Xu and Zhang [37] solved surface modeling problems using sixth-order nonlinear geometric flow.

In this paper, we generate triply periodic constant mean curvature surfaces with various volume fractions using a phase-field model. Our proposed algorithm allows us to generate a phase-field whose zero level set is a constant mean curvature surface. Like the

* Corresponding author.
E-mail addresses: sdyang@korea.ac.kr (S.-D. Yang), leeh@korea.ac.kr (H.G. Lee), cfdkim@korea.ac.kr (J. Kim).
URL: http://www.math.korea.ac.kr/~cfdkim/ (J. Kim).

0010-4655/$ – see front matter
doi:10.1016/j.cpc.2010.02.010

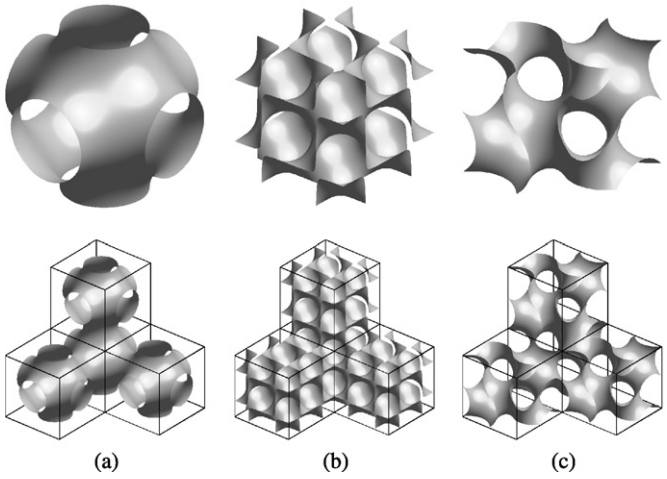

Fig. 1. Three different minimal surfaces: (a) Schwarz P (primitive), (b) Schwarz D (diamond), and (c) Schoen G (gyroid) surface.

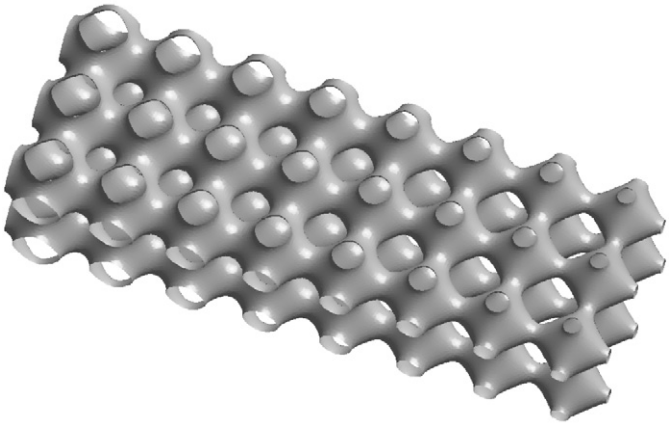

Fig. 2. Variable porosity structure.

level set method, a phase-field can express two phases. Generated phase-field can be applied to a wide range of problems: designing biomedical scaffolds [9] (see Fig. 2), solving numerically partial differential equations on surfaces [12], analyzing fluid flow with surfaces [18].

This paper is organized as follows. In Section 2, we present of the phase-field formulation for surface area minimization in the presence of a volume fraction constraint. In Section 3, an unconditionally gradient stable numerical scheme described. In Section 4, numerical results are presented. We give some concluding remarks in Section 5. In Appendix A, the fully discrete nonlinearly gradient stable scheme and its multigrid solver are given.

2. Phase-field formulation

2.1. The variational problem

Our exploration of triply periodic surfaces that are local minima of the total interfacial area subject to a volume constraint is based on a phase-field model. Following the usual methodology, we represent a surface as the one-half level set of an embedding function, $\phi(x, y, z)$, defined throughout the three-dimensional domain and use variational calculus to derive the relationship between ϕ and global geometric properties of the surface.

In this section, we present a detailed discussion of the phase-field formulation for surface area minimization in the presence of a volume fraction constraint. In the present discussion, we derive

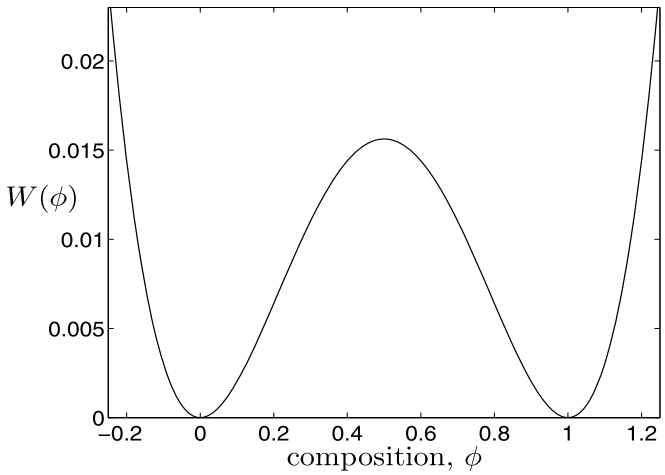

Fig. 3. A double well potential, $W(\phi) = 0.25\phi^2(1-\phi)^2$.

formulas for the area and volume of a triply periodic surface and the variations of these quantities with respect to ϕ.

For the triply periodic problems that we are interested in, the domain Ω is taken to be a unit cube and the surface of interest is represented by the one-half level set of ϕ. That is,

$$\Omega = [0,1]^3 \quad \text{and} \quad \Gamma = \left\{ (x,y,z) \in \Omega \colon \phi(x,y,z) = \frac{1}{2} \right\}.$$

Then Γ divides the unit cell into two distinct phases. Without loss of generality, we define the region where $\phi(\mathbf{x}) > 1/2$ to be phase 1. In terms of the embedding function, ϕ, our minimization problem may be stated as

$$\text{minimize } \mathcal{A}(\phi) \quad \text{subject to} \quad V(\phi) = V_{\frac{1}{2}},$$

where $\mathcal{A}(\phi)$ is the total surface area of the one-half level set and $V(\phi)$ is the volume fraction of phase 1, i.e.,

$$V(\phi) := \frac{\text{volume of the region with } \phi > 1/2}{\text{total volume of the region}} \tag{1}$$

and $V_{1/2}$ is the desired volume fraction for phase 1.

2.2. The Cahn–Hilliard equation

Our exploration of triply-periodic surfaces that are local minima of the total interfacial area subject to a volume constraint is based on ideas underlying the application of the phase-field method to spinodal decomposition. Important features of the phase-field method for these studies are that fast solvers exist for the numerical integration of the Cahn–Hilliard equation and time accurate intermediate solutions are obtained.

We start with the free energy functional written in terms of the local volume fraction ϕ as

$$\mathcal{F}(\phi) = 6\sqrt{2} \int_\Omega \left[\frac{1}{\epsilon} W(\phi) + \frac{\epsilon}{2} |\nabla \phi|^2 \right] d\mathbf{x}, \tag{2}$$

where $W(\phi) = 0.25\phi^2(1-\phi)^2$ is the double well potential as shown in Fig. 3.

The coefficient ϵ is a small positive constant. The time-evolution equation with volume fraction conservation for ϕ is given by [8].

$$\frac{\partial \phi}{\partial t} = M \Delta \mu, \tag{3}$$

where M is a mobility and

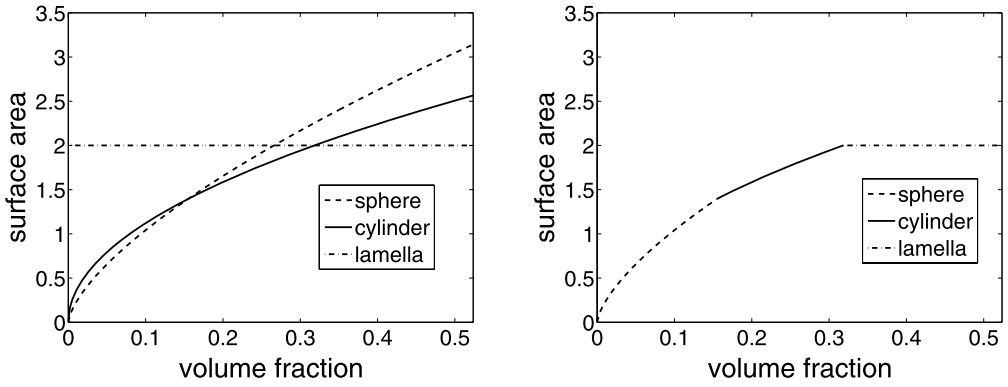

Fig. 4. (a) The spheres, cylinders, and planes profile in Ω. (b) The spheres–cylinders–planes profile in Ω.

$$\mu := \frac{\delta \mathcal{F}}{\delta \phi} = 6\sqrt{2}\left[\frac{1}{\epsilon}W'(\phi) - \epsilon\Delta\phi\right] = 6\sqrt{2}\left[\frac{1}{\epsilon}\left(\phi^3 - \frac{3}{2}\phi^2 + \frac{1}{2}\phi\right) - \epsilon\Delta\phi\right].$$

By differentiation of the energy $\mathcal{F}(\phi)$ and the total mass $\int_\Omega \phi\, d\mathbf{x}$, we see that

(1) the total energy is non-increasing and
(2) the total mass is conserved, i.e.,

$$\frac{d\mathcal{F}}{dt} = 6\sqrt{2}\int_\Omega \left[\frac{1}{\epsilon}W'(\phi)\phi_t + \epsilon\nabla\phi\cdot\nabla\phi_t\right] d\mathbf{x} = \int_\Omega \mu\phi_t\, d\mathbf{x} = \int_\Omega \mu M\Delta\mu\, d\mathbf{x} = -M\int_\Omega |\nabla\mu|^2\, d\mathbf{x} \leqslant 0$$

and

$$\frac{d}{dt}\int_\Omega \phi\, d\mathbf{x} = \int_\Omega \phi_t\, d\mathbf{x} = \int_\Omega M\Delta\mu\, d\mathbf{x} = \int_{\partial\Omega} M\frac{\partial\mu}{\partial n}\, ds = 0,$$

where we have used the triply periodic boundary conditions. We define

$$\mathcal{A}(\phi) := \int_\Omega 6\sqrt{2}\epsilon|\nabla\phi|^2\, d\mathbf{x},$$

which is related to $\mathcal{F}(\phi)$ by $\mathcal{A}(\phi)\sim\mathcal{F}(\phi)$ when the phase-field ϕ is in equilibrium, i.e., when $W(\phi) = \frac{\epsilon^2}{2}|\nabla\phi|^2$. $\mathcal{F}(\phi)$ approaches the surface area when $\epsilon\to 0+$. So a critical point of $\mathcal{F}(\phi)$ is expected to approach a critical point of the area functional as $\epsilon\to 0+$. For later use we record that for any v such that $\int_\Omega v\, d\mathbf{x} = 0$,

$$\begin{aligned}\left.\frac{d\mathcal{F}(\phi+\eta v)}{d\eta}\right|_{\eta=0} &= \left.\frac{d}{d\eta}6\sqrt{2}\int_\Omega\left[\frac{1}{\epsilon}W(\phi+\eta v) + \frac{\epsilon}{2}|\nabla(\phi+\eta v)|^2\right]d\mathbf{x}\right|_{\eta=0}\\ &= 6\sqrt{2}\int_\Omega\left[\frac{1}{\epsilon}W'(\phi)v + \epsilon\nabla\phi\cdot\nabla v\right]d\mathbf{x}\\ &= 6\sqrt{2}\int_\Omega\left[\frac{1}{\epsilon}W'(\phi) - \epsilon\Delta\phi\right]v\, d\mathbf{x} + 6\sqrt{2}\int_{\partial\Omega}\epsilon v\frac{\partial\phi}{\partial n}\, ds\\ &= \int_\Omega \mu v\, d\mathbf{x}. \end{aligned} \tag{4}$$

2.3. Periodic isoperimetric problem for different volume fraction

A full result characterizing all global minimizers of the periodic isoperimetric problem in $\mathbb{R}^n$ $(n\geqslant 3)$ for different volume fraction remains an open problem in classical geometry [5]. However, in triply periodic surfaces, the conjecture is well accepted and well tested [14,29]. Conjecture: global minimizers of triply periodic surfaces are either a sphere, a cylinder, or two parallel planes for a cubic flat torus $\mathbb{T}^3$.

We define the spheres–cylinders–planes profile (scp profile) of Ω as the function $I_{scp}:(0,\pi/6)\to\mathbb{R}^+$ which gives the least area among spheres, cylinders, and pairs of parallel planes enclosing a volume V [14]. From the graphs (Fig. 4(a)), we have that (see Fig. 4(b)).

$$I_{scp}(V) = \begin{cases} (36\pi V^2)^{1/3} & \text{if } 0 < V \leqslant \frac{4\pi}{81},\\ 2\sqrt{\pi V} & \text{if } \frac{4\pi}{81}\leqslant V\leqslant\frac{1}{\pi},\\ 2 & \text{if } \frac{1}{\pi}\leqslant V. \end{cases}$$

2.4. Local minimization of the functional

In order to find a local minima of the functional equation (2) we calculate an equilibrium solution ϕ to Eq. (3). Suppose ϕ is an equilibrium solution to Eq. (3). Then using the fact that $\Delta\mu = 0$ and that μ is periodic in all three directions, we have

$$\int_\Omega |\nabla\mu|^2\, d\mathbf{x} = \int_{\partial\Omega}\mu\frac{\partial\mu}{\partial n}\, ds - \int_\Omega \mu\Delta\mu\, d\mathbf{x} = 0.$$

Therefore, $\nabla\mu = (0,0,0)$, hence μ is constant. Therefore, we see from Eq. (4) that for any v such that $\int_\Omega v\, d\mathbf{x} = 0$,

$$\left.\frac{d\mathcal{F}(\phi+\eta v)}{d\eta}\right|_{\eta=0} = \mu\int_\Omega v\, d\mathbf{x} = 0.$$

Thus, ϕ is a critical point of $\mathcal{F}(\phi)$. Conversely, suppose that ϕ is a critical point of $\mathcal{F}(\phi)$. Then from Eq. (4)

$$\int_\Omega \mu v\, d\mathbf{x} = \left.\frac{d\mathcal{F}(\phi+\eta v)}{d\eta}\right|_{\eta=0} = 0$$

for any $\int_\Omega v\,d\mathbf{x}=0$. Let $\alpha=\int_\Omega \mu\,d\mathbf{x}/\int_\Omega d\mathbf{x}$ be the average of μ over the domain, Ω. Next we choose $v=\mu-\alpha$, then $\int_\Omega v\,d\mathbf{x}=0$, hence

$$0=\int_\Omega \mu v\,d\mathbf{x}=\int_\Omega (\mu-\alpha)v\,d\mathbf{x}=\int_\Omega (\mu-\alpha)^2\,d\mathbf{x}.$$

Therefore, $\mu=\alpha$ is constant, and, since ϕ satisfies Eq. (3) from the beginning, ϕ is an equilibrium solution to Eq. (3).

2.5. The mean curvature of the level set

Given $\phi:\mathbb{R}^3\to\mathbb{R}$, suppose that the level set $\Gamma=\{(x,y,z)\in\mathbb{R}^3:\ \phi(x,y,z)=\frac{1}{2}\}$ is a C^2 surface. Then, the mean curvature of the surface is

$$H=-\frac{1}{2}\nabla\cdot\mathbf{n}$$

where $\nabla=(\partial_x,\partial_y,\partial_z)$ and $\mathbf{n}=\frac{\nabla\phi}{|\nabla\phi|}$ [25].

Now suppose that $\phi:\Omega\to\mathbb{R}$ which is an equilibrium solution of Eq. (2) and that the level surface $\Gamma=\{(x,y,z):\ \phi(x,y,z)=0\}$ of the phase-field function is a C^2 surface. We further assume that for all $\mathbf{x}\in\Omega$

$$\phi(\mathbf{x})=q\left(\frac{d(\mathbf{x})}{2\sqrt{2}\epsilon}\right)+g(\mathbf{x}),\quad \text{where } q:\mathbb{R}\to\mathbb{R}\quad\text{and}$$

$$q(t):=\frac{1}{2}(1+\tanh t),$$

$d:\Omega\to\mathbb{R}$ is the signed distance between $\mathbf{x}$ and Γ, positive in one side and negative in the other side, and $\|\nabla^k g\|_{L^{\inf}}=o(\epsilon)$ for $k=0,\dots,4$ [6]. Note that Γ now coincides with the zero level set of d. From

$$q'=2q(1-q),\qquad q''=4q(1-q)(1-2q),\qquad |\nabla d|=1,$$

$$\nabla\phi\sim\frac{q'}{2\sqrt{2}\epsilon}\nabla d,\qquad \Delta\phi\sim\frac{q''}{8\epsilon^2}+\frac{q'}{2\sqrt{2}\epsilon}\Delta d,$$

we have

$$\begin{aligned}-2H=\nabla\cdot\left(\frac{\nabla d}{|\nabla d|}\right)=\Delta d&\sim\frac{2\sqrt{2}\epsilon}{q'}\left(\Delta\phi-\frac{q''}{8\epsilon^2}\right)\\&=\frac{\sqrt{2}\epsilon}{q(1-q)}\left[\Delta\phi-\frac{q(1-q)(1-2q)}{2\epsilon^2}\right]\\&=\frac{\sqrt{2}\epsilon}{\phi(1-\phi)}\left[\Delta\phi-\frac{\phi(1-\phi)(1-2\phi)}{2\epsilon^2}\right]\\&=-\frac{1}{6\phi(1-\phi)}\mu,\end{aligned}$$

which results in $H\sim\mu/3$ on the one-half level set Γ of a local equilibrium solution ϕ. Since μ is constant on the one-half level set of ϕ, we conclude that the mean curvature is constant on Γ as $\epsilon\to 0+$.

3. Unconditionally gradient stable numerical scheme

Since we want to calculate long time evolution, we use an unconditionally gradient stable scheme [7,8,19,35]. In the rest of this article, we fix the mobility $6\sqrt{2}M/\epsilon$ to be 1. The resulting time-stepping is:

$$\frac{\phi_{ijk}^{n+1}-\phi_{ijk}^{n}}{\Delta t}=\Delta_d v_{ijk}^{n+1}-\frac{1}{4}\Delta_d\phi_{ijk}^{n},\tag{5}$$

$$v_{ijk}^{n+1}=f\left(\phi_{ijk}^{n+1}\right)-\epsilon^2\Delta_d\phi_{ijk}^{n+1},\tag{6}$$

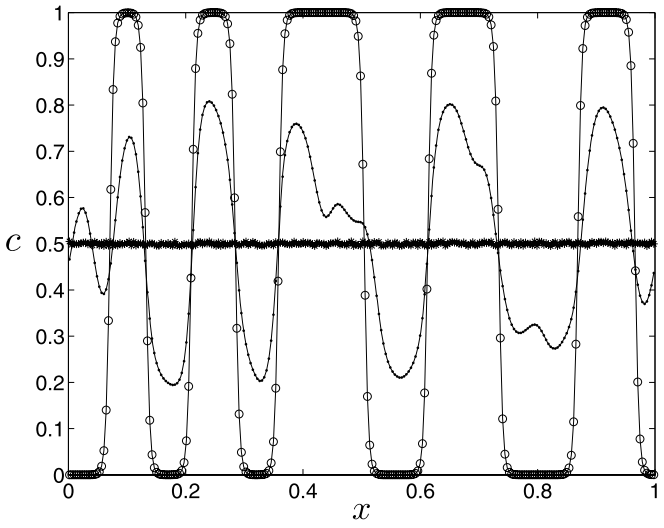

Fig. 5. The evolution of an initial random distribution of concentration, $c(x,0)=0.5+0.01\,\mathrm{rand}(x)$. The concentration profile is shown at $t=0$ ('∗'), 0.3 ('·'), and 10 ('∘').

where the nonlinear function $f(\phi)=\phi^3-\frac{3}{2}\phi^2+\frac{3}{4}\phi$. All structures we have investigated are periodic. Thus periodicity had to be incorporated into Eqs. (5) and (6). It was done by periodic boundary conditions

$$\phi_{0jk}=\phi_{Njk},\qquad \phi_{N+1,jk}=\phi_{1jk},\qquad \phi_{i0k}=\phi_{iNk},$$

$$\phi_{i,N+1,k}=\phi_{i1k},\qquad \phi_{ij0}=\phi_{ijN},\qquad \phi_{ij,N+1}=\phi_{ij1}$$

and similarly with v. The above discrete system is solved by a nonlinear multigrid method. Numerical solution is described in Appendix A. We define a discrete l_2-norm as follow

$$\|\phi\|=\sqrt{\frac{1}{N^3}\sum_{i,j,k=1}^{N}\phi_{ijk}^2}.$$

We will compare our results from a phase-field method with ones from the level set method.

4. Numerical results

In this section, we present numerical results showing efficiency and accuracy of the proposed method. In particular, we describe the algorithm to generate constant mean curvature surfaces with volume constraint using a phase-field model.

4.1. The relation between the ϵ value and the width of the transition layer

In our first numerical experiment, we consider the relation between the ϵ value and the width of the transition layer. From our choice of the total energy density and an equilibrium profile $c(x)=\tanh(x/(2\sqrt{2}\epsilon))$ on the infinite domain, the concentration field varies from 0.1 to 0.9 over a distance of about $4\sqrt{2}\epsilon\tanh^{-1}(0.9)$. Therefore, if we want this value to be about m grid points, then

$$\epsilon_m=\frac{hm}{4\sqrt{2}\tanh^{-1}(0.9)}.$$

To confirm this, we ran a simulation with the initial condition $c(x,0)=0.5+0.01\,\mathrm{rand}(x)$ on the unit domain $\Omega=(0,1)$ with $h=1/128$, $\Delta t=0.05$, and ϵ_4 (see the line with stars in Fig. 5). Here, $\mathrm{rand}(x)$ is a random number between -1 and 1. In Fig. 5, we see that the transition layer (from $c=0.1$ to $c=0.9$) is about 4 grid points at time $t=10$.

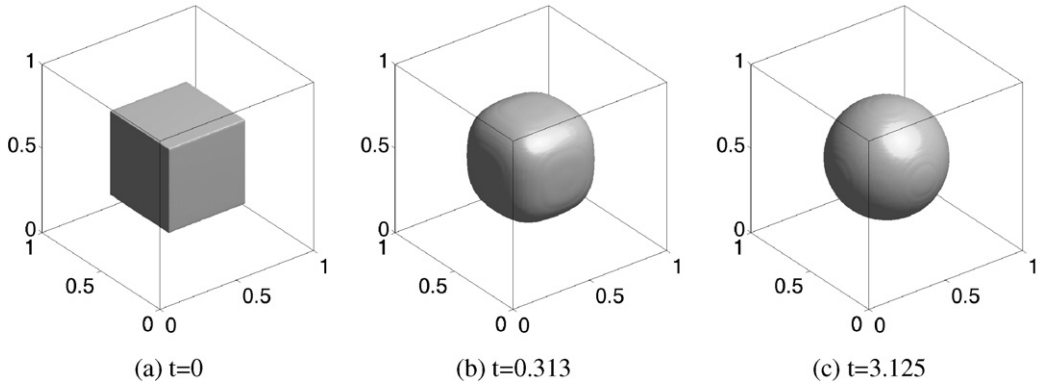

Fig. 6. Evolution of a cube surface to the locally optimal sphere surface.

Table 1
Convergence results – surface area and total mean curvature with $r = 0.25$.

Mesh	32^3	Rate	64^3	Rate	128^3	Rate	256^3
Surface area	0.42403	1.56	0.66323	1.35	0.73742	1.56	0.76923
Total mean curvature	2.25072	1.87	2.89797	1.74	3.06842	3.71	3.13601

4.2. Verification of numerical optimization algorithm

To verify our numerical optimization algorithm, we tested its ability to accurately compute a structure whose local optimality is easily verified. The test case is the sphere. It is a locally optimal surface. In this test, we started the optimization algorithm with a cube as the initial surface.

$$\phi^0(x, y, z) = \begin{cases} 1 & \text{if } 0.25 \leqslant x, y, z \leqslant 0.75, \\ 0 & \text{otherwise.} \end{cases}$$

Fig. 6 shows that the cube evolves to the sphere, as expected. This result was computed on the computational domain $\Omega = (0, 1) \times (0, 1) \times (0, 1)$ with a mesh 64^3, $h = 1/64$, $\Delta t = h$, and $\epsilon = 0.015$.

4.3. Convergence test

To check the convergence of the scheme, we perform a number of simulations on increasingly finer grids. The initial state for this convergence test on a domain, $\Omega = (0, 1) \times (0, 1) \times (0, 1)$, is

$$\phi^0(x, y, z) = \frac{1}{2}\left(1 + \tanh\left(\frac{0.25 - \sqrt{(x-0.5)^2 + (y-0.5)^2 + (z-0.5)^2}}{2\sqrt{2}\epsilon}\right)\right).$$

The numerical solutions are computed on the uniform grids, $h = 1/2^n$ for $n = 5, 6, 7$, and 8. For each case, the calculation is run with $\Delta t = h$ and $\epsilon = 0.0073 \times 64/2^n$. We stop the numerical computations when the discrete l_2-norm of the difference between $(n+1)$th and nth time step solutions becomes less than 10^{-5}. That is $\|\phi^{n+1} - \phi^n\| \leqslant 10^{-5}$. We define the error e_h to be the difference between theoretical and numerical values. The rate of convergence is defined as: $\log_2(e_h/e_{h/2})$. The results and rates of convergence are given in Table 1. The results suggest that the scheme is first and higher order accurate.

4.4. Algorithm for generating constant mean curvature surfaces

There are many known ways to compute the Schwarz P, Schwarz D, and Schoen G triply periodic minimal surfaces. They can be characterized exactly using the Enneper–Weierstrass representation [25], generated as the local minima of the scalar order parameter Landau–Ginzburg functional used to describe ordering phenomena in microemulsions [11], and approximated by Fourier series using the periodic nodal surface (PNS) expansion [10,22,30,31].

In this section, we examine three families of surfaces with the symmetry and topology as the Schwarz P, Schwarz D, and Schoen G surfaces but with different values for the volume fraction of phase 1. The minimization procedure requires an initial configuration. We generated initial configurations with the desired symmetry, topology, and volume fractions by taking the following PNS approximations of the Schwarz P, Schwarz D, and Schoen G surfaces [10]:

$$P(x, y, z) = \cos 2\pi x + \cos 2\pi y + \cos 2\pi z + 0.5, \tag{7}$$

$$D(x, y, z) = \cos 2\pi x \cos 2\pi y \cos 2\pi z - \sin 2\pi x \sin 2\pi y \sin 2\pi z + 0.5, \tag{8}$$

$$G(x, y, z) = \sin 2\pi x \cos 2\pi y + \sin 2\pi z \cos 2\pi x + \sin 2\pi y \cos 2\pi z + 0.5. \tag{9}$$

Note that the leading term only PNS equations (7)–(9) are neither minimal nor constant mean curvature surfaces [23]. Now, we describe our new algorithm for generating constant mean curvature surfaces. For clarity of exposition, let us consider one-dimensional version of the Schwarz P surface,

$$\phi_i^{\text{step } 1} = \cos 2\pi x_i + 0.5 \quad \text{for } i = 1, \ldots, N. \tag{10}$$

In Fig. 7, the solid line represents $\phi^{\text{step } 1}$ in Eq. (10).

Next, truncate non-physical values such as negative and greater than one values. For $i = 1, \ldots, N$,

$$\phi_i^{\text{step } 2} = \begin{cases} 1 & \text{if } \phi_i^{\text{step } 1} > 1, \\ 0 & \text{if } \phi_i^{\text{step } 1} < 0, \\ \phi_i^{\text{step } 1} & \text{otherwise.} \end{cases} \tag{11}$$

In Fig. 7, the dashed line shows $\phi^{\text{step } 2}$ in Eq. (11). Then we evolve $\phi^{\text{step } 2}$ with 5ϵ by solving Eqs. (5) and (6) to get $\phi^{\text{step } 3}$. Typically, we take five time step iterations. In Fig. 7, the line with the symbol '$\circ$' shows the evolved $\phi^{\text{step } 3}$.

Given a phase-field ϕ, a volume fraction α, and a parameter β, we define the average volume fraction $V_{ave}(\phi, \alpha, \beta)$ as

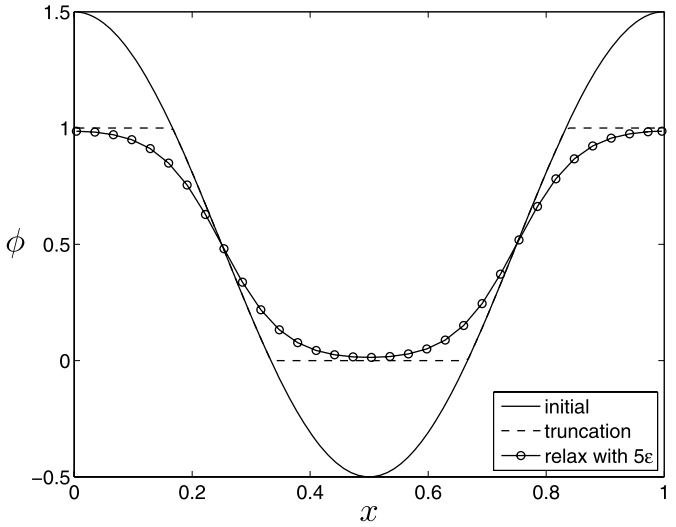

Fig. 7. $\phi^{\text{step 1}}$ ('—'), $\phi^{\text{step 2}}$ ('- -'), and $\phi^{\text{step 3}}$ ('-○-').

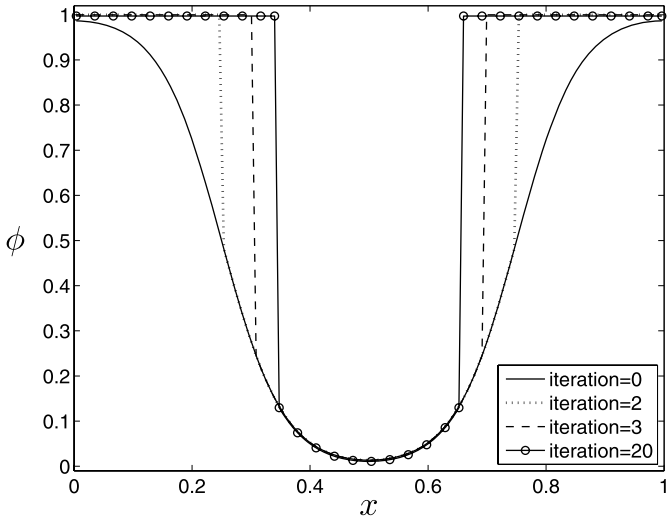

Fig. 8. The evolution of the phase-field by the bisection algorithm is illustrated.

$$V_{ave}(\phi,\alpha,\beta)=\frac{1}{N}\sum_{i=1}^{N}\tilde{\phi}_i,$$

where in the case of $\alpha>0.5$, $\tilde{\phi}_i=1$ if $\phi_i>\beta$ and $\tilde{\phi}_i=\phi_i$ otherwise, and in the case of $\alpha\leqslant 0.5$, $\tilde{\phi}_i=0$ if $\phi_i<\beta$ and $\tilde{\phi}_i=\phi_i$ otherwise.

Taking different β values, we can generate various average volume fractions within a prescribed tolerance. To find an approximate solution to $V_{ave}(\phi,\alpha,\beta)=\alpha$ with a given volume fraction α on the interval $[0,1]$ with tolerance *tol* and maximum number of iteration *max_it*, we take the following bisection algorithm [3].

Begin algorithm
Let $f(x)=V_{ave}(\phi,\alpha,x)-\alpha$, $\beta_1=0$, and $fa=f(\beta_1)$.
if $|fa|<tol$, then return β_1
else
  set $k=2$, $a=0$, $b=1$
  while $(k\leqslant max\_it)$ do
    $\beta_k=a+(b-a)/2$ and $fp=f(\beta_k)$
    if $|fp|<tol$ or $(b-a)/2<tol$, then return β_k and exit while loop
    else
      set $k=k+1$
      If $fa\cdot fp>0$, then set $a=\beta_k$ and $fa=fp$
      else set $b=\beta_k$.
      end if
    end if
  end while
end if
End algorithm

We define the phase-field $\phi^{\text{step 4}}$ with the returned value of β_k; i.e., in the case $\alpha>0.5$,

$$\phi_i^{\text{step 4}}=\begin{cases}1 & \text{if } \phi_i^{\text{step 3}}>\beta_k,\\ \phi_i^{\text{step 3}} & \text{otherwise,}\end{cases}$$

and in the case of $\alpha\leqslant 0.5$,

$$\phi_i^{\text{step 4}}=\begin{cases}0 & \text{if } \phi_i^{\text{step 3}}<\beta_k,\\ \phi_i^{\text{step 3}} & \text{otherwise.}\end{cases}$$

In Fig. 8, the evolutions by the method described in the above bisection algorithm are shown and the converged result is $\phi^{\text{step 4}}$. In Fig. 9(a), lines with the symbols, '○' and '⋆', denote $V_{ave}(\phi,0.7,\beta_k)$ and β_k at each iteration of the above algorithm, respectively.

Since $V_{ave}(\phi,\alpha,\beta_k)$ is equal to α within the tolerance we adjust volume fraction by shifting $\phi_i^{\text{step 4}}$.

$$\phi_i^{\text{step 5}}=\phi_i^{\text{step 4}}+\alpha-\frac{1}{N}\sum_{k=1}^{N}\phi_k^{\text{step 4}}\quad\text{for } i=1,\ldots,N.$$

Finally, we evolve $\phi^{\text{step 5}}$ with ϵ by solving Eqs. (5) and (6) to get $\phi^{\text{step 6}}$ (see Fig. 9(b)). The above procedures are summarized as follows:

$$\text{PNS}\left(\phi^{\text{step 1}}\right)\xrightarrow{\text{truncation}}\phi^{\text{step 2}}\xrightarrow{\text{relax with }5\epsilon}\phi^{\text{step 3}}$$
$$\xrightarrow{\text{bisection}}\phi^{\text{step 4}}\xrightarrow{\text{shifting}}\phi^{\text{step 5}}\xrightarrow{\text{relax with }\epsilon}\phi^{\text{step 6}}.$$

We can apply the same approach to three-dimensional cases and to other surfaces such as $D(x,y,z)$ and $G(x,y,z)$ with a straightforward procedure. In Fig. 10, (a) $\phi^{\text{step 3}}$ and (b) $\phi^{\text{step 6}}$ of P (top), D (middle), and G (bottom) surfaces are shown. Volume fractions of (a) and (b) are $\alpha=0.5$ and $\alpha=0.7$, respectively. The gray, dark gray, and black iso-surfaces represent level surfaces at $\phi=0.3$, 0.5, and 0.7, respectively.

4.5. Local equilibrium surfaces of the Schwarz P, Schwarz D, and Schoen G surfaces families

In this section, we perform the procedures described in Section 4.4 for the following volume fractions: 0.25, 0.3, 0.35, 0.4, 0.45, 0.5, 0.55, 0.6, 0.65, 0.7, and 0.75. For these calculations, we employed the computational domain $\Omega=(0,1)\times(0,1)\times(0,1)$ with a mesh 256^3, $h=1/256$, $\Delta t=0.5h$, and $\epsilon=0.01$. We stop the numerical computations when the difference between $(n+1)$th and nth time step areas becomes less than 10^{-6}. That is $|\mathcal{A}(\phi^{n+1})-\mathcal{A}(\phi^n)|\leqslant 10^{-6}$. Fig. 11 shows results of our proposed algorithm with those obtained by Y. Jung et al. [17] using the level set method. In Fig. 11, (a) mean curvature versus volume fraction and (b) total surface area per unit cell versus volume fraction for local equilibrium surfaces of P, D, and G surfaces families are shown. For these calculations, the computational times, reaching the stopping criterion for P, D, and G surfaces, took approximately 10, 12, and 7 h on a single computer, respectively. The results from phase-field model show excellent agreement with the results of Y. Jung et al. And although we used the higher grid resolution than that of the calculations by Y. Jung et al. and simulated on a single computer (cf. in [17], simulations were run for

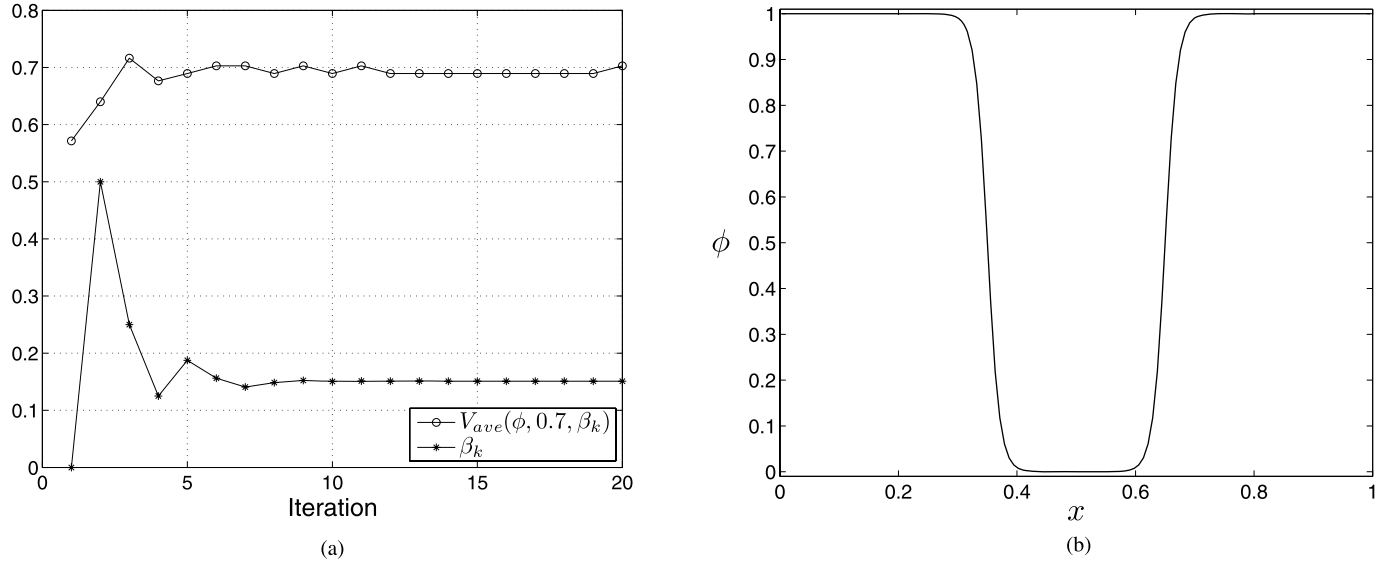

(a) (b)

Fig. 9. (a) Lines with the symbols, '○' and '⋆', denote $V_{ave}(\phi, 0.7, \beta_k)$ and β_k at each iteration of the bisection method, respectively. (b) The final numerical solution, $\phi^{\text{step } 6}$.

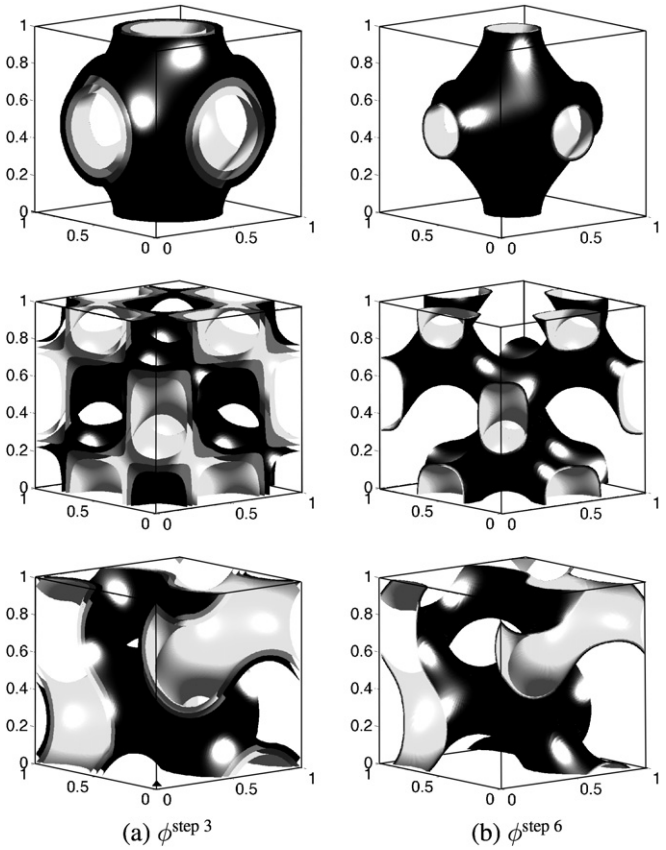

Fig. 10. (a) $\phi^{\text{step } 3}$ and (b) $\phi^{\text{step } 6}$ of P (top), D (middle), and G (bottom) surfaces. Volume fractions of (a) and (b) are $\alpha = 0.5$ and $\alpha = 0.7$, respectively. The gray, dark gray, and black iso-surfaces represent level surfaces at $\phi = 0.3$, 0.5, and 0.7, respectively.

a 4 node parallel calculation on the Opteron cluster), we reached the stopping criterion faster than Y. Jung et al. (see Table 2). Note that the P, D, and G minimal surfaces are globally not of absolute minimum area; in fact, minimal surfaces of P, D, and G are of local maximum areas within their families as shown in Fig. 11(b) [15].

Table 2
Comparison of the performance of phase-field and level-set methods.

Case	TPMS	Phase-field	Level-set
Tolerance of the stopping criterion	P surface	10^{-6}	10^{-6}
	D surface	10^{-6}	10^{-5}
	G surface	10^{-6}	N/A
Hardware that used for calculations	All surfaces	Single computer	4 node parallel calculations on the Opteron cluster
Mesh size	P surface	$256 \times 256 \times 256$	$200 \times 200 \times 200$
	D surface	$256 \times 256 \times 256$	$250 \times 250 \times 250$
	G surface	$256 \times 256 \times 256$	$200 \times 200 \times 200$
Computational time	P surface	10 h	29 h
	D surface	12 h	30 h
	G surface	7 h	N/A

5. Conclusions

In this paper, we presented an accurate and efficient algorithm to generate constant mean curvature surfaces with volume constraint using a phase-field model. Starting from the periodic nodal surface approximation to minimal surfaces, we could generate the Schwarz primitive (P), Schwarz diamond (D), and Schoen gyroid (G) surfaces with various volume fractions. We compared the results from our proposed algorithm with the results from the level set method and found excellent agreement. This technique for generating constant mean curvature surfaces has a potential to be used for designing biomedical scaffolds with optimal mechanical and biomorphic properties. In the future work, we will investigate the Allen–Cahn equation with a penalty to generate constant mean curvature surfaces with volume constraint.

Acknowledgements

S.-D. Yang was supported in part by a research grant from the College of Science at Korea University. J.S. Kim was supported by Basic Science Research Program through the National Research Foundation of Korea (NRF) funded by the Ministry of Education, Science and Technology (2009-0086388). The authors are grateful to Professor Do Wan Kim for his suggestions, comments, and valuable inputs of the manuscript.

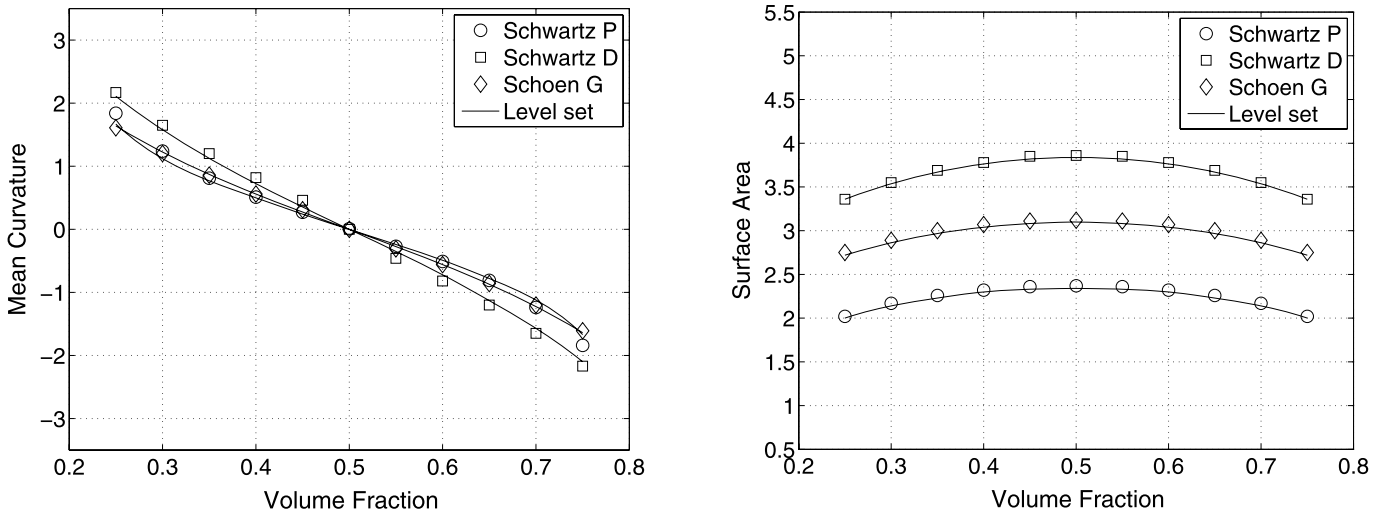

(a) (b)

Fig. 11. (a) Mean curvature versus volume fraction and (b) total surface area per unit cell versus volume fraction for local equilibrium surfaces of the Schwarz P, Schwarz D, and Schoen G surfaces families.

Appendix A. Numerical solution

In this section, we develop a nonlinear Full Approximation Storage (FAS) multigrid method to solve the nonlinear discrete system (5) and (6) at the implicit time level. The nonlinearity is treated using one step of Newton's iteration and a pointwise Gauss–Seidel relaxation scheme is used as the smoother in the multigrid method. See the reference text [34] for additional details and background. The algorithm of the nonlinear multigrid method for solving the discrete CH system is: First, let us rewrite Eqs. (5) and (6) as follows.

$$NSO\left(\phi^{n+1}, \nu^{n+1}\right) = \left(\varphi^n, \psi^n\right),$$

where

$$NSO\left(\phi^{n+1}, \nu^{n+1}\right) = \left(\frac{\phi^{n+1}}{\Delta t} - \Delta_d \nu^{n+1}, -f\left(\phi^{n+1}\right) + \epsilon^2 \Delta_d \phi^{n+1} + \nu^{n+1}\right)$$

and the source term is $(\varphi^n, \psi^n) = (\phi^n/\Delta t - 0.25\Delta_d \phi^n, 0)$.

In the following description of one FAS cycle, we assume a sequence of grids Ω_l (Ω_{l-1} is coarser than Ω_l by factor 2). Given the number β of pre- and post-smoothing relaxation sweeps, an iteration step for the nonlinear multigrid method using the V-cycle is formally written as follows [34]:

FAS multigrid cycle

$$\left\{\phi_l^{m+1}, \nu_l^{m+1}\right\} = FAScycle\left(l, \phi_l^m, \nu_l^m, NSO_l, \varphi_l^n, \psi_l^n, \beta\right).$$

That is, $\{\phi_l^m, \nu_l^m\}$ and $\{\phi_l^{m+1}, \nu_l^{m+1}\}$ are the approximations of $\phi^{n+1}(x_i, y_j, z_k)$ and $\nu^{n+1}(x_i, y_j, z_k)$ before and after an *FAScycle*. Now, define the *FAScycle*.

1) Presmoothing

$$\left\{\bar{\phi}_l^m, \bar{\nu}_l^m\right\} = SMOOTH^{\beta}\left(\phi_l^m, \nu_l^m, NSO_l, \varphi_l^n, \psi_l^n\right),$$

which means performing β smoothing steps with the initial approximations ϕ_l^m, ν_l^m, source terms φ_l^n, ψ_l^n, and *SMOOTH* relaxation operator to get the approximations $\bar{\phi}_l^m, \bar{\nu}_l^m$. One *SMOOTH* relaxation operator step consists of solving the system (A.3) and (A.4) given below by 2×2 matrix inversion for each i, j, and k. Here, we derive the smoothing operator in three dimensions. Rewriting Eq. (5), we get

$$\frac{\phi_{ijk}^{n+1}}{\Delta t} + \frac{6\nu_{ijk}^{n+1}}{h^2} = \varphi_{ijk}^n + \left(\nu_{i+1,j,k}^{n+1} + \nu_{i-1,j,k}^{n+1} + \nu_{i,j+1,k}^{n+1} + \nu_{i,j-1,k}^{n+1} + \nu_{i,j,k+1}^{n+1} + \nu_{i,j,k-1}^{n+1}\right)/h^2. \tag{A.1}$$

Since $f(\phi_{ijk}^{n+1})$ is nonlinear with respect to ϕ_{ijk}^{n+1}, we linearize $f(\phi_{ijk}^{n+1})$ at ϕ_{ijk}^m, i.e.,

$$f\left(\phi_{ijk}^{n+1}\right) \approx f\left(\phi_{ijk}^m\right) + \frac{df\left(\phi_{ijk}^m\right)}{d\phi}\left(\phi_{ijk}^{n+1} - \phi_{ijk}^m\right).$$

After substitution of this into Eq. (6), we get

$$\begin{aligned} &-\left(\frac{df\left(\phi_{ijk}^m\right)}{d\phi} + \frac{6\epsilon^2}{h^2}\right)\phi_{ijk}^{n+1} + \nu_{ijk}^{n+1} \\ &\quad = \psi_{ijk}^n + f\left(\phi_{ijk}^m\right) - \frac{df\left(\phi_{ijk}^m\right)}{d\phi}\phi_{ijk}^m \\ &\qquad - \frac{\epsilon^2}{h^2}\left(\phi_{i+1,j,k}^{n+1} + \phi_{i-1,j,k}^{n+1} + \phi_{i,j+1,k}^{n+1} + \phi_{i,j-1,k}^{n+1} \right. \\ &\qquad \left. + \phi_{i,j,k+1}^{n+1} + \phi_{i,j,k-1}^{n+1}\right). \end{aligned} \tag{A.2}$$

Next, we replace $\phi_{ii,jj,kk}^{n+1}$ and $\nu_{ii,jj,kk}^{n+1}$ in Eqs. (A.1) and (A.2) with $\bar{\phi}_{ii,jj,kk}^m$ and $\bar{\nu}_{ii,jj,kk}^m$ if $ii \leqslant i$, $jj \leqslant j$, and $kk \leqslant k$, otherwise with $\phi_{ii,jj,kk}^m$ and $\nu_{ii,jj,kk}^m$, i.e.,

$$\frac{\bar{\phi}_{ijk}^m}{\Delta t} + \frac{6\bar{\nu}_{ijk}^m}{h^2} = \varphi_{ijk}^n + \left(\nu_{i+1,j,k}^m + \bar{\nu}_{i-1,j,k}^m + \nu_{i,j+1,k}^m + \bar{\nu}_{i,j-1,k}^m + \nu_{i,j,k+1}^m + \bar{\nu}_{i,j,k-1}^m\right)/h^2, \tag{A.3}$$

$$\begin{aligned} &-\left(\frac{df\left(\phi_{ijk}^m\right)}{d\phi} + \frac{6\epsilon^2}{h^2}\right)\bar{\phi}_{ijk}^m + \bar{\nu}_{ijk}^m \\ &\quad = \psi_{ijk}^n + f\left(\phi_{ijk}^m\right) - \frac{df\left(\phi_{ijk}^m\right)}{d\phi}\phi_{ijk}^m \\ &\qquad - \frac{\epsilon^2}{h^2}\left(\phi_{i+1,j,k}^m + \bar{\phi}_{i-1,j,k}^m + \phi_{i,j+1,k}^m + \bar{\phi}_{i,j-1,k}^m \right. \\ &\qquad \left. + \phi_{i,j,k+1}^m + \bar{\phi}_{i,j,k-1}^m\right). \end{aligned} \tag{A.4}$$

2) Compute the defect

$$\left(\bar{d}_{1\,l}^m, \bar{d}_{2\,l}^m\right) = \left(\varphi_l^n, \psi_l^n\right) - NSO_l\left(\bar{\phi}_l^m, \bar{\nu}_l^m\right).$$

3) Restrict the defect and $\{\bar{\phi}_l^m, \bar{v}_l^m\}$

$$\left(\bar{d}_{1\,l-1}^m, \bar{d}_{2\,l-1}^m\right) = I_l^{l-1}\left(\bar{d}_{1\,l}^m, \bar{d}_{2\,l}^m\right),$$
$$\left(\bar{\phi}_{l-1}^m, \bar{v}_{l-1}^m\right) = I_l^{l-1}\left(\bar{\phi}_l^m, \bar{v}_l^m\right).$$

The restriction operator I_l^{l-1} maps l-level functions to $(l-1)$-level functions.

$$\begin{aligned} d_{l-1}(x_i, y_j, z_k) &= I_l^{l-1} d_l(x_i, y_j, z_k) \\ &= \frac{1}{8}\big[d_l(x_{i-\frac{1}{2}}, y_{j-\frac{1}{2}}, z_{k-\frac{1}{2}}) + d_l(x_{i-\frac{1}{2}}, y_{j-\frac{1}{2}}, z_{k+\frac{1}{2}}) \\ &\quad + d_l(x_{i-\frac{1}{2}}, y_{j+\frac{1}{2}}, z_{k-\frac{1}{2}}) + d_l(x_{i-\frac{1}{2}}, y_{j+\frac{1}{2}}, z_{k+\frac{1}{2}}) \\ &\quad + d_l(x_{i+\frac{1}{2}}, y_{j-\frac{1}{2}}, z_{k-\frac{1}{2}}) + d_l(x_{i+\frac{1}{2}}, y_{j-\frac{1}{2}}, z_{k+\frac{1}{2}}) \\ &\quad + d_l(x_{i+\frac{1}{2}}, y_{j+\frac{1}{2}}, z_{k-\frac{1}{2}}) + d_l(x_{i+\frac{1}{2}}, y_{j+\frac{1}{2}}, z_{k+\frac{1}{2}})\big]. \end{aligned}$$

4) Compute the right-hand side

$$\left(\varphi_{l-1}^n, \psi_{l-1}^n\right) = \left(\bar{d}_{1\,l-1}^m, \bar{d}_{2\,l-1}^m\right) + NSO_{l-1}\left(\bar{\phi}_{l-1}^m, \bar{v}_{l-1}^m\right).$$

5) Compute an approximate solution $\{\hat{\phi}_{l-1}^m, \hat{v}_{l-1}^m\}$ *of the coarse grid equation on* Ω_{l-1}*, i.e.*

$$NSO_{l-1}\left(\phi_{l-1}^m, v_{l-1}^m\right) = \left(\varphi_{l-1}^n, \psi_{l-1}^n\right). \tag{A.5}$$

If $l = 1$, we apply the smoothing procedure in 1) to obtain the approximate solution. If $l > 1$, we solve Eq. (A.5) by performing an FAS l-grid cycle using $\{\bar{\phi}_{l-1}^m, \bar{v}_{l-1}^m\}$ as an initial approximation:

$$\begin{aligned} &\left\{\hat{\phi}_{l-1}^m, \hat{v}_{l-1}^m\right\} \\ &\quad = FAScycle\left(l-1, \bar{\phi}_{l-1}^m, \bar{v}_{l-1}^m, NSO_{l-1}, \varphi_{l-1}^n, \psi_{l-1}^n, \beta\right). \end{aligned}$$

6) Compute the coarse grid correction (CGC):

$$\hat{v}_{1l-1}^m = \hat{\phi}_{l-1}^m - \bar{\phi}_{l-1}^m, \qquad \hat{v}_{2l-1}^m = \hat{v}_{l-1}^m - \bar{v}_{l-1}^m.$$

7) Interpolate the correction: $\hat{v}_{1l}^m = I_{l-1}^l \hat{v}_{1l-1}^m$, $\hat{v}_{2l}^m = I_{l-1}^l \hat{v}_{2l-1}^m$.

Here, the coarse values are simply transferred to the eight nearby fine grid points, i.e., $v_l(x_i, y_j, z_k) = I_{l-1}^l v_{l-1}(x_i, y_j, z_k) = v_{l-1}(x_{i+\frac{1}{2}}, y_{j+\frac{1}{2}}, z_{k+\frac{1}{2}})$ for i, j, and k odd-numbered integers.

8) Compute the corrected approximation on Ω_l

$$\phi_l^{m,\text{after } CGC} = \bar{\phi}_l^m + \hat{v}_{1l}^{\,m}, \qquad v_l^{m,\text{after } CGC} = \bar{v}_l^m + \hat{v}_{2l}^{\,m}.$$

9) Postsmoothing

$$\begin{aligned} &\left\{\phi_l^{m+1}, v_l^{m+1}\right\} \\ &\quad = SMOOTH^{\beta}\left(\phi_l^{m,\text{after } CGC}, v_l^{m,\text{after } CGC}, NSO_l, \varphi_l^n, \psi_l^n\right). \end{aligned}$$

This completes the description of a nonlinear FAScycle.

Appendix B. Discretization of the surface area and the surface averaged total curvature

In this section, we derive discretizations of the surface area and the surface averaged total curvature.

Vertex-centered normal vectors are obtained by differentiating the phase-field in the eight surrounding cells. For example, the normal vector at the top right back vertex of cell Ω_{ijk} is given by

$$\mathbf{m}_{i+\frac{1}{2},j+\frac{1}{2},k+\frac{1}{2}} = \left(m^x_{i+\frac{1}{2},j+\frac{1}{2},k+\frac{1}{2}}, m^y_{i+\frac{1}{2},j+\frac{1}{2},k+\frac{1}{2}}, m^z_{i+\frac{1}{2},j+\frac{1}{2},k+\frac{1}{2}}\right),$$

where

$$\begin{aligned} m^x_{i+\frac{1}{2},j+\frac{1}{2},k+\frac{1}{2}} &= \frac{\phi_{i+1,j,k} + \phi_{i+1,j,k+1} + \phi_{i+1,j+1,k} + \phi_{i+1,j+1,k+1}}{4h} \\ &\quad - \frac{\phi_{ijk} + \phi_{i,j,k+1} + \phi_{i,j+1,k} + \phi_{i,j+1,k+1}}{4h} \end{aligned}$$

and other terms are defined similarly. The curvature is calculated at cell centers from the vertex-centered normals and is given by

$$\begin{aligned} \kappa(\phi_{ijk}) &= \nabla_d \cdot \left(\frac{\mathbf{m}}{|\mathbf{m}|}\right)_{ijk} \\ &= \frac{1}{4h}\Bigg(\frac{m^x_{i+\frac{1}{2},j+\frac{1}{2},k+\frac{1}{2}} + m^y_{i+\frac{1}{2},j+\frac{1}{2},k+\frac{1}{2}} + m^z_{i+\frac{1}{2},j+\frac{1}{2},k+\frac{1}{2}}}{|\mathbf{m}_{i+\frac{1}{2},j+\frac{1}{2},k+\frac{1}{2}}|} \\ &\quad + \frac{m^x_{i+\frac{1}{2},j+\frac{1}{2},k-\frac{1}{2}} + m^y_{i+\frac{1}{2},j+\frac{1}{2},k-\frac{1}{2}} - m^z_{i+\frac{1}{2},j+\frac{1}{2},k-\frac{1}{2}}}{|\mathbf{m}_{i+\frac{1}{2},j+\frac{1}{2},k-\frac{1}{2}}|} \\ &\quad + \frac{m^x_{i+\frac{1}{2},j-\frac{1}{2},k+\frac{1}{2}} - m^y_{i+\frac{1}{2},j-\frac{1}{2},k+\frac{1}{2}} + m^z_{i+\frac{1}{2},j-\frac{1}{2},k+\frac{1}{2}}}{|\mathbf{m}_{i+\frac{1}{2},j-\frac{1}{2},k+\frac{1}{2}}|} \\ &\quad + \frac{m^x_{i+\frac{1}{2},j-\frac{1}{2},k-\frac{1}{2}} - m^y_{i+\frac{1}{2},j-\frac{1}{2},k-\frac{1}{2}} - m^z_{i+\frac{1}{2},j-\frac{1}{2},k-\frac{1}{2}}}{|\mathbf{m}_{i+\frac{1}{2},j-\frac{1}{2},k-\frac{1}{2}}|} \\ &\quad - \frac{m^x_{i-\frac{1}{2},j+\frac{1}{2},k+\frac{1}{2}} - m^y_{i-\frac{1}{2},j+\frac{1}{2},k+\frac{1}{2}} - m^z_{i-\frac{1}{2},j+\frac{1}{2},k+\frac{1}{2}}}{|\mathbf{m}_{i-\frac{1}{2},j+\frac{1}{2},k+\frac{1}{2}}|} \\ &\quad - \frac{m^x_{i-\frac{1}{2},j+\frac{1}{2},k-\frac{1}{2}} - m^y_{i-\frac{1}{2},j+\frac{1}{2},k-\frac{1}{2}} + m^z_{i-\frac{1}{2},j+\frac{1}{2},k-\frac{1}{2}}}{|\mathbf{m}_{i-\frac{1}{2},j+\frac{1}{2},k-\frac{1}{2}}|} \\ &\quad - \frac{m^x_{i-\frac{1}{2},j-\frac{1}{2},k+\frac{1}{2}} + m^y_{i-\frac{1}{2},j-\frac{1}{2},k+\frac{1}{2}} - m^z_{i-\frac{1}{2},j-\frac{1}{2},k+\frac{1}{2}}}{|\mathbf{m}_{i-\frac{1}{2},j-\frac{1}{2},k+\frac{1}{2}}|} \\ &\quad - \frac{m^x_{i-\frac{1}{2},j-\frac{1}{2},k-\frac{1}{2}} + m^y_{i-\frac{1}{2},j-\frac{1}{2},k-\frac{1}{2}} + m^z_{i-\frac{1}{2},j-\frac{1}{2},k-\frac{1}{2}}}{|\mathbf{m}_{i-\frac{1}{2},j-\frac{1}{2},k-\frac{1}{2}}|}\Bigg), \end{aligned}$$

where $\nabla_d \cdot$ is a finite difference approximation to the divergence operator. And the cell-centered normal is the average of vertex normals,

$$\begin{aligned} \nabla_d \phi_{ijk} = \Bigg(&\frac{\phi_{i-2,j,k} - 8\phi_{i-1,j,k} + 8\phi_{i+1,j,k} - \phi_{i+2,j,k}}{12h}, \\ &\frac{\phi_{i,j-2,k} - 8\phi_{i,j-1,k} + 8\phi_{i,j+1,k} - \phi_{i,j+2,k}}{12h}, \\ &\frac{\phi_{i,j,k-2} - 8\phi_{i,j,k-1} + 8\phi_{i,j,k+1} - \phi_{i,j,k+2}}{12h}\Bigg), \end{aligned}$$

where ∇_d is a finite difference approximation to the gradient operator. Therefore, the discretization of the surface area $\mathcal{A}$ is

$$\mathcal{A}(\phi) = \sum_{i,j,k=1}^{N} 6\sqrt{2}\epsilon |\nabla_d \phi_{ijk}|^2 h^3$$

and the surface averaged total curvature is

$$\bar{\kappa}(\phi) = -\frac{\sum_{i,j,k=1}^{N} 6\sqrt{2}\epsilon \kappa(\phi_{ijk}) |\nabla_d \phi_{ijk}|^2 h^3}{\mathcal{A}(\phi)}.$$

And therefore the surface averaged mean curvature is

$$\bar{H}(\phi) = -\frac{1}{2}\bar{\kappa}(\phi).$$

References

[1] O. Alexandrov, F. Santosa, J. Comput. Phys. 204 (2005) 121.
[2] K. Brakke, Experiment. Math. 1 (1992) 141.
[3] R.L. Burden, J.D. Faires, Numerical Analysis, Thomson, 2004.
[4] M. do Carmo, Differential Geometry of Curves and Surfaces, Prentice Hall, 1976.
[5] R. Choksi, P. Sternberg, Interfaces Free Bound. 8 (2006) 371.
[6] Q. Du, C. Liu, R. Ryham, X. Wang, Nonlinearity 18 (2005) 1249.
[7] D. Eyre, An unconditionally stable one-step scheme for gradient systems, http://www.math.utah.edu/~eyre/research/methods/stable.ps.
[8] D. Eyre, in: Computational and Mathematical Models of Microstructural Evolution, 1998, p. 39.
[9] R. Gabbrielli, I.G. Turner, C.R. Bowen, Key Eng. Mater. Bioceramics 20 (2008) 903.
[10] P.J.F. Gandy, S. Bardhan, A.L. Mackay, J. Klinowski, Chem. Phys. Lett. 336 (2001) 187.
[11] W.T. Góźgź, R. Holyst, Phys. Rev. Lett. 76 (1996) 2726.
[12] J.B. Greer, A.L. Bertozzi, G. Sapiro, J. Comput. Phys. 216 (2006) 216.
[13] K. Grosse-Brauckmann, J. Colloid Interface Sci. 187 (1997) 418.
[14] L. Hauswirth, J. Perez, P. Romon, A. Ros, Trans. Amer. Math. Soc. 356 (2004) 2025.
[15] S. Hildebrandt, A. Tromba, Mathematics and Optimal Form, Scientific American Library, 1985.
[16] S.T. Hyde, Curr. Opin. Solid State Mater. Sci. 1 (1996) 653.
[17] Y. Jung, K.T. Chu, S. Torquato, J. Comput. Phys. 223 (2007) 711.
[18] Y. Jung, S. Torquato, Phys. Rev. E 72 (2005) 056319-1.
[19] J. Kim, H. Bae, J. Korean Phys. Soc. 53 (2008) 672.
[20] J. Klinowski, A.L. Mackay, H. Terrones, Phil. Trans. R. Soc. Lond. A 354 (1996) 1975.
[21] E.A. Lord, A.L. Mackay, Current Sci. 85 (2003) 346.
[22] A.L. Mackay, Proc. R. Soc. Lond. A 442 (1993) 47.
[23] A.L. Mackay, Chem. Phys. Lett. 221 (1994) 317.
[24] National Research Council, Biomolecular Self-Assembling Materials: Scientific and Technological Frontiers, National Academies Press, 1996.
[25] J.C.C. Nitsche, Introduction, Fundamentals, Geometry and Basic Boundary Value Problems, Lectures on Minimal Surfaces, vol. 1, Cambridge University Press, 1989.
[26] S.J. Osher, R.P. Fedkiw, Level Set Methods and Dynamic Implicit Surfaces, Springer-Verlag, 2002.
[27] S.J. Osher, F. Santosa, J. Comput. Phys. 171 (2001) 272.
[28] S. Rajagopalan, R.A. Robb, Lecture Notes in Comput. Sci. 3749 (2005) 794.
[29] A. Ros, The isoperimetric problem, in: Proceedings of the Clay Mathematics Institute Summer School on the Global Theory of Minimal Surfaces, 2001, http://www.ugr.es/~aros/isoper.htm.
[30] H.G. von Schnering, R. Nesper, Z. Phys. B: Condens. Matter 83 (1991) 407.
[31] U.S. Schwarz, G. Gompper, Phys. Rev. E 59 (1999) 5528.
[32] J.A. Sethian, Level Set Methods and Fast Marching Methods: Evolving Interfaces in Computational Geometry, Fluid Mechanics, Computer Vision, and Materials Science, Cambridge University Press, 1999.
[33] E.J. Siem, W.C. Carter, Interface Sci. 10 (2002) 287.
[34] U. Trottenberg, C. Oosterlee, A. Schüller, MULTIGRID, Academic Press, 2001.
[35] B.P. Vollmayr-Lee, A.D. Rutenberg, Phys. Rev. E 68 (2003) 066703-1.
[36] Y. Wang, Computer-Aided Design 39 (2007) 179.
[37] G. Xu, Q. Zhang, Computer-Aided Design 39 (2007) 342.